Line Tension and Line Entropy Associated with the Monolayer/Trilayer Boundary of Smectic Liquid Crystal at the Air-Water Interface

*Huda A. Alwusaydi[1,2], Joseph S. Yarzebinski[2], Pritam Mandal[2], J. Adin Mann Jr[3] and Elizabeth K. Mann[2]**

[1]Department of Physics and Astronomy, King Saud University, Riyadh, Saudi Arabia, [2]Department of Physics, Kent State University, Kent, OH, [3] Department of Chemical and Biomolecular Engineering, Case Western Reserve University, Cleveland, OH

ABSTRACT: Molecularly thin films of the smectic liquid crystal 4′-octyl-4-biphenylcarbonitrile (8CB) at the air-water interface phase separate into regions with different numbers of layers, in analogy with free-standing smectic liquid crystalline films. This study reports the line tension associated with the boundary of coexisting trilayer and monolayer phases of in Langmuir films of 8CB at the air-water interface as a function of temperature and humidity and infers information on the boundary profile between the coexisting phases. Two complementary techniques were used to characterize the 8CB thin films: surface pressure/area isotherm and Brewster Angle Microscopy (BAM). We determine the line tension by stretching isolated domains from their equilibrium circular shape and analyzing the free relaxation with a hydrodynamic model. Then, we interpret the line tension vs. temperature data in terms of an excess line entropy for the domain boundary,

which requires careful consideration of the thermodynamics of inhomogeneous monolayer systems.

I. INTRODUCTION

Analogous to the surface tension associated with the interface of two bulk phases in a three-dimensional system, line tension is defined as the line excess energy per unit boundary length at the boundary between two phases within a quasi-two-dimensional film. Line tension between coexisting phases has been considered to play a potential role in governing dynamic functional domains within cell membranes, sometimes called lipid rafts [1-9]. These nanodomains are thought to have significant roles in cell signaling and membrane-protein trafficking within biological membranes. [10-14].

Line tension is one key parameter that governs and modulates the shape, size and dynamics of the domains. The competition between the line tension (short-range attraction) at the boundary of the domain and dipolar repulsion between molecular dipoles aligned by the interface determines the equilibrium domain size and shape [15-21]. On the other hand, the presence of long-range repulsion would complicate the measurement and understanding of the bare line tension. Further, this repulsion is thought to be much less important for cell membranes because the bilayer structure reduces the net dipole moment.

Here, we study the effect of temperature on the line tension in a much simpler model system, consisting of coexisting monolayer and trilayer domains in a Langmuir film (a layer, one or a few molecules thick, of amphiphilic molecules trapped at the gas/liquid interface) of the smectic liquid crystal 4′-octyl-4-biphenylcarbonitrile (8CB) at the air/water interface. In this case, dipolar repulsion is minimized due to the symmetry of the bilayer on top of the monolayer. This is confirmed by the small contrast in the electrostatic potential between the two phases [20,22].

Further, multiple studies of the liquid crystal 8CB in free standing films [23,24] and in Langmuir films [21,22] have measured the line tension at constant temperature as a function of the thickness jump across the boundary. These studies suggest that the shape of the boundary profile, and the energy between two fluid phases within the surface film, are determined by minimizing the combined energies associated with the core defect, layer distortion and two independent surfaces [23,24]. Furthermore, Zou and coworkers showed that the line tension within 8CB multilayers at the air-water interface is linearly dependent on the film thickness, which suggests a smooth transition between two different discrete phases over a boundary zone with a characteristic length scale. For trilayer/monolayer coexistence, the length scale was estimated to be ~ 28 nm, equivalent to about 15 8CB molecules [22]. Note that this length scale is much larger than the width of a typical liquid/fluid interface, which is of the order of 1 molecule.

We present line tension data of two coexisting liquid phases across a temperature range corresponding to different bulk phases, from the crystalline to the nematic. We investigate the temperature dependence of the trilayer/monolayer line tension to deduce more information about the configuration of the domain boundary, which is difficult to find by direct measurements. We expect an excess disorder associated with the line, leading to a decrease in line tension with temperature. Therefore, we interpret the line tension as a function of temperature in terms of line entropy per unit length. Interpretation requires carefully defining line excess quantities, in analogy to surface excess quantities.

Various methods have been developed to measure line tension, including using domain boundary fluctuations [5], shape distributions [4] and domain relaxation dynamics [20,22]. The domain edge fluctuation method is most appropriate for small line tensions where the amplitude of the fluctuations is relatively large, so that the fluctuations are clearly visible with an optical

microscope. This technique is not suitable for our system with larger values of line tension [5]. The shape distribution method is also not appropriate because the theory behind this method requires an equilibrium distribution of domain size to provide accurate line tension values, and that equilibrium may be hard to obtain [4].

Here, we use domain relaxation dynamics, through the quantitative analysis of a deformed domain relaxing back to its energy-minimizing circular shape, to determine the line tension. The line tension is the driving force, opposed by the subfluid viscosity, for the relaxation process. A manageable mathematical model of relaxation phenomena, developed by Bernoff and coworkers [25,26], which involves two coexisting planar liquid phases on an incompressible subfluid, is used to determine the line tension. The model reduces the differential formulation, with both bulk and surface Naviers-Stokes equations as well as boundary conditions at both the surface and the line, to a more tractable non-dimensional boundary integral formulation [25-27]. More details are given in the methods section.

A. Surface and line thermodynamics

The thermodynamics of the line can be treated in the same fashion as that of the interface in which the line is embedded. The surface thermodynamics of thin films was first developed by Gibbs [28]. We follow the treatment developed by Hansen [29] and Turkevich and J.A Mann [30].

As shown in Figure 1a, the system consists of a two-dimensional fluid with two separate liquid phases of different thicknesses at the air-water interface. The Gibbs convention, which is a convenient method of defining both surface and line excess quantities, is used. To do so, both the interfacial surface between the two bulk phases (Air and water) and the line boundary between phase-separated domains in a pure monolayer must be carefully defined (Figure 1b). We introduce the Gibbs dividing surface that imposes zero surface excess water. Note that the Gibbs dividing

surface is drawn slightly above the line defining the bottom edge of the monolayer (Figure 1c), as water is expected to penetrate into the film headgroup region.

Next, the Gibbs dividing line between trilayer and monolayer phases is defined, applying a similar convention of zero line excess of 8CB, as shown in FIG. 1.

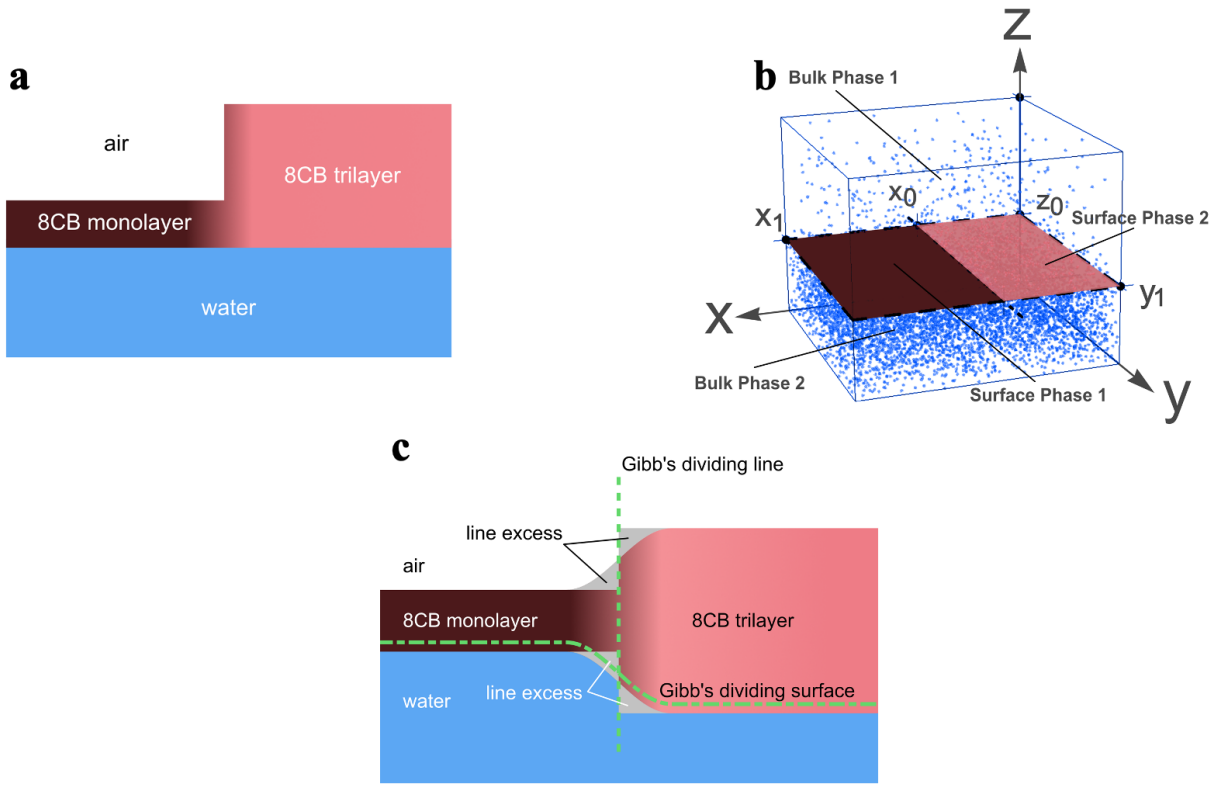

FIG. 1. Defining the Gibbs dividing surface and line for trilayer/monolayer coexisting phases at the air/water interface. (a) Simplified model of the film. (b) Three-dimensional model showing the Gibbs dividing surface and the Gibbs dividing line. (c) Cross section of the profile of 8CB layer showing the Gibbs dividing surface and line.

The defined boundary surface and line separate the bulk, surface and line quantities, which are separately in equilibrium. Thus, the Gibbs-Duhem relation for the system as a whole [28]:

$$0 = SdT - VdP + N_{water}\, d\mu_{water} + N_{8CB}\, d\mu_{8CB} + Ld\lambda + Ad\gamma, \qquad (1)$$

can be written in terms of separate surface and line terms as follows

$$0= \left(S^{(b)} + S^{(s)} + S^{(l)}\right)dT - VdP + \left({N_{water}}^{(b)} + {N_{water}}^{(s)} + {N_{water}}^{(l)}\right)d\mu_{water} + \left({N_{8CB}}^{(S)} + {N_{8CB}}^{(l)}\right)d\mu_{8CB} + Ld\lambda + Ad\gamma, \quad (2)$$

where $S^{(b)}, S^{(s)}, S^{(l)}$ are bulk, surface and line entropies, ${N_{water}}^{(b)}, {N_{water}}^{(s)}, {N_{water}}^{(l)}$ are the number bulk, surface, and line water molecules, ${N_{8CB}}^{(S)}$, ${N_{8CB}}^{(l)}$ are the number of surface and line 8CB molecules, and γ, λ are surface and line tension respectively. Here, the amount of 8CB in bulk is not included because 8CB molecules are trapped at the interface.

These equations must hold true separately for the bulk, surface, and line. Thus, the surface Gibbs-Duhem equation (Eq. (2)) at constant pressure can be written as

$$0= S^{(s)}dT + {N_{water}}^{(s)}d\mu_{water} + {N_{8CB}}^{(S)}d\mu_{8CB} + Ad\gamma, \quad (3)$$

and using the Gibbs convention, the excess surface entropy is given by [28-30]

$$S^s \equiv \frac{S}{A} = -\frac{d\gamma}{dT}, \quad (4)$$

where γ is the surface tension and T is the temperature of the substrate.

Similarly, the line Gibbs-Duhem equation can be given as

$$0= S^{(L)}dT + {N_{water}}^{(L)}\, d\mu_{water} + {N_{8CB}}^{(L)}d\mu_{8CB} + \lambda dL \quad (5)$$

and the excess line entropy can then be written as

$$S^L \equiv \frac{S}{L} = -\frac{d\lambda}{dT}. \quad (6)$$

II. MATERIAL AND METHOD

B. Materials

Line tension experiments requires high purity for all materials. If even trace contaminants are line active, they would concentrate at the monolayer/trilayer boundary and change its line tension. Two different sources of 8CB material and two different troughs were used to test the

purity of the system, as any impurities were highly likely to be different in the four cases. 8CB samples, with chemical structure shown in FIG. 2, were purchased from Sigma Aldrich, 98% ALDRICH, (sample 1) and BDH Ltd (sample 2 &3). 8CB was dissolved in hexane, OPTIMA™ grade purchased from Fisher, to obtain solution with concentrations between 0.20 and 0.30 mg/mL. Ultra-pure water produced by a PURELAB® Ultra water system (Seimans, resistivity 18.2 M Ω/cm, TOC<2 ppb, passes the bubble test) was used as substrate.

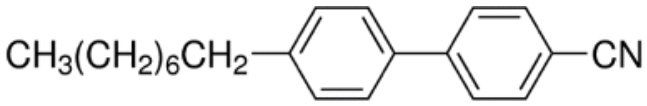

FIG. 2. Chemical structure of 4′-octyl-4-biphenylcarbonitrile (8CB).

C. Experimental setup

The Langmuir technique is used (KSV instruments) with two different types of troughs in order to access the whole range of the temperature (10-50℃): one is a rectangular (364 mm ×75 mm) KSV Langmuir minitrough which is made of solid Teflon™ sitting on the top of aluminum base; the Teflon delaminated from the base at higher temperatures, so that a different design is required in this limit. The other is a circular trough (inner radius =54 mm, outer radius = 68 mm, depth = 68 mm), which is fabricated in aluminum and coated with black Teflon™ by E.L. Stone Company, Inc. (Norton, OH.). The depth of this trough helps trap the laser beam [31].

To facilitate the temperature control of the subphase, two different sets of heating systems are used, depending on the trough; A Julabo™ water bath circulates hot or cold water through the base of the minitrough. Electric cartridge heaters, connected to a temperature controller, fit into holes in the sides of the aluminum trough [32]. A thermistor gives direct readings of subphase

temperature. Both systems control the temperature with a precision of ±0.2 ℃ ; the water bath can both heat and cool the minitrough while the cartridge heater system can only heat the aluminum one.

While the cylindrical trough allowed us to achieve temperatures to 50 ℃ and higher, it did not allow us to use barriers for compression/decompression of the film. Therefore, for consistency, the desired concentration was reached by successive addition in all of these experiments .

These troughs are carefully cleaned with a dilute, easily rinsed soap solution (Extran™ 300 Detergent), then rinsed three or more times with deionized water, and finally with ultra-pure water. This cleaning is essential to remove any dust or organic molecules and obtain data with high accuracy. The ultrapure water is used as the subphase. Then, a spreading solution of 8CB in the hexane with concentrations between 0.20 and 0.30 mg/mL, is carefully deposited using a Hamilton syringe on the pure water in a well-cleaned trough. The hexane evaporates, leaving 8CB molecules spread over the subphase. The surface pressure is monitored by a Wilhelmy plate with a precision of ± 0.2 mN/m. To control the surface concentration, we use the method of successive addition, waiting a minimum of ten minutes for the evaporation of hexane before any measurements.

The surface is imaged using a homemade [34] Brewster Angle Microscope [35]. For 8CB on water, there is no sign of any in-plane anisotropy of the 8CB films, consistent with earlier measurements [22,36]. Therefore, brighter domains imply thicker ones.

D. 2.3 Determining the line tension

In order to measure the line tension associated with coexisting monolayer and trilayer domains, we use hydrodynamic shear to stretch an 8CB domain. The shear flow is induced using a platinum wire (diameter=1.3mm) to stir the substrate. Once the shear dies down, after ~ 5 s, the domain relaxes to the energy-minimizing circular shape, driven by line tension. Typically, the

domain is stretched sufficiently that it is still deformed at that time. Stirring too fast causes fluid flow sufficient to drive the relaxing domain out the field of view, while stirring too slowly is insufficient to significantly stretch the domains. Further, only domains that are far apart from each other are analyzed, to reduce the hydrodynamic effects from neighboring domains. Neighboring domains significantly affect the relaxation process of the domain of interest and are not accounted for in our model.

The relaxation event is recorded in AVI video files. A series of images with their real (experimental) time are cut from the video file using the "Premiere Pro CC" program. Then, the images are fit to a hydrodynamic model for distorted domains relaxing to circular ones, using software developed by the Bernoff group [25-26]. This software simulates the relaxation as it proceeds in non-dimensional time, T, defined by the following equation [25-27]

$$T = \frac{t}{T^*}, \qquad T^* = \frac{\eta(T)A}{\lambda} \tag{7}$$

where $\eta(T)$ is the viscosity of water, A area of the domain (A), and T^* is the characteristic time used to make the hydrodynamic equations non-dimensional.

This software first traces the boundaries of the domain in each image. It then uses the distorted shape of the first image as an initial condition. The simulated time T is then related linearly to the real time t as shown in FIG. 3 through the characteristic time T^* (the slope of the curve), which allows one to directly extract the line tension from Eq. (7).

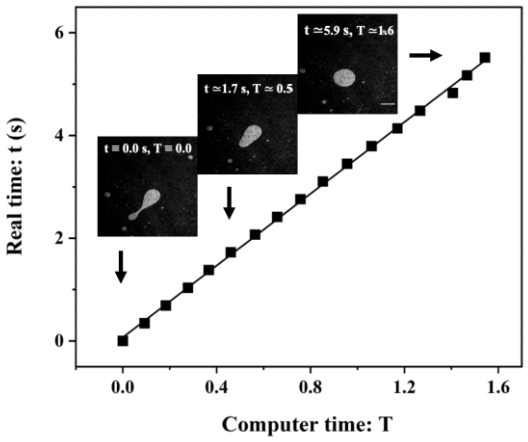

FIG. 3. The real time vs. simulated time and raw images of domain relaxation of a trilayer domain (light gray domain) on top of the 8CB monolayer (background) through Brewster Angle Microscope. Scale bare $200\mu m$.

The characteristic relaxation time T^* increases with viscosity, while it decreases with increasing line tension, the driving force, and with decreasing area, corresponding to higher radii of curvature and larger Laplace pressures [25,26]. The linear relationship between the simulated and experimental times shown in FIG. 3 is an excellent test of the underlying hydrodynamic model. With isolated domains, a quiescent bulk during relaxation, and a clean surface, the line tension obtained in this model has a much smaller uncertainty, ~1%, compared to earlier uncertainties, which were ~20% [15,21].

III. RESULTS

E. The surface excess entropy

FIG. 4 shows the surface pressure vs. mean molecular area isotherm of 8CB at the air-water interface. The isotherm was consistent with the reported literature [36-38]. The isotherm indicates different phases analogous to bulk phases. For a few 8CB molecules at the surface, the coexisting

gas and liquid monolayer phases forms with almost zero surface pressure as shown in FIG. 4a. With more material added or with more compression, the monolayer first covers the whole surface as seen in FIG. 4b and then the surface pressure steeply increases. As the monolayer is further compressed beyond the mean molecular area A= 0.40 nm^2, trilayer islands appear and grow within the monolayer (FIG. 4c), at a single surface pressure value around ~ 5mN/m. At this point, further addition or compression of 8CB results in a full trilayer that covers the whole surface of the subphase. Thereafter, the trilayer collapses to multilayers phases, consisting of integer numbers of bilayers on top of the trilayer, shown in FIG. 4d. The contrasts between the two coexisting phases were enhanced, especially in FIG. 4 a and c, to make the domains and their edges more visible. The brightest areas in Figure 4a are close in intensity to the darkest areas of FIG. 4c, while the brightest areas in FIG 4c are close in intensity to the darkest areas in FIG. 4d.

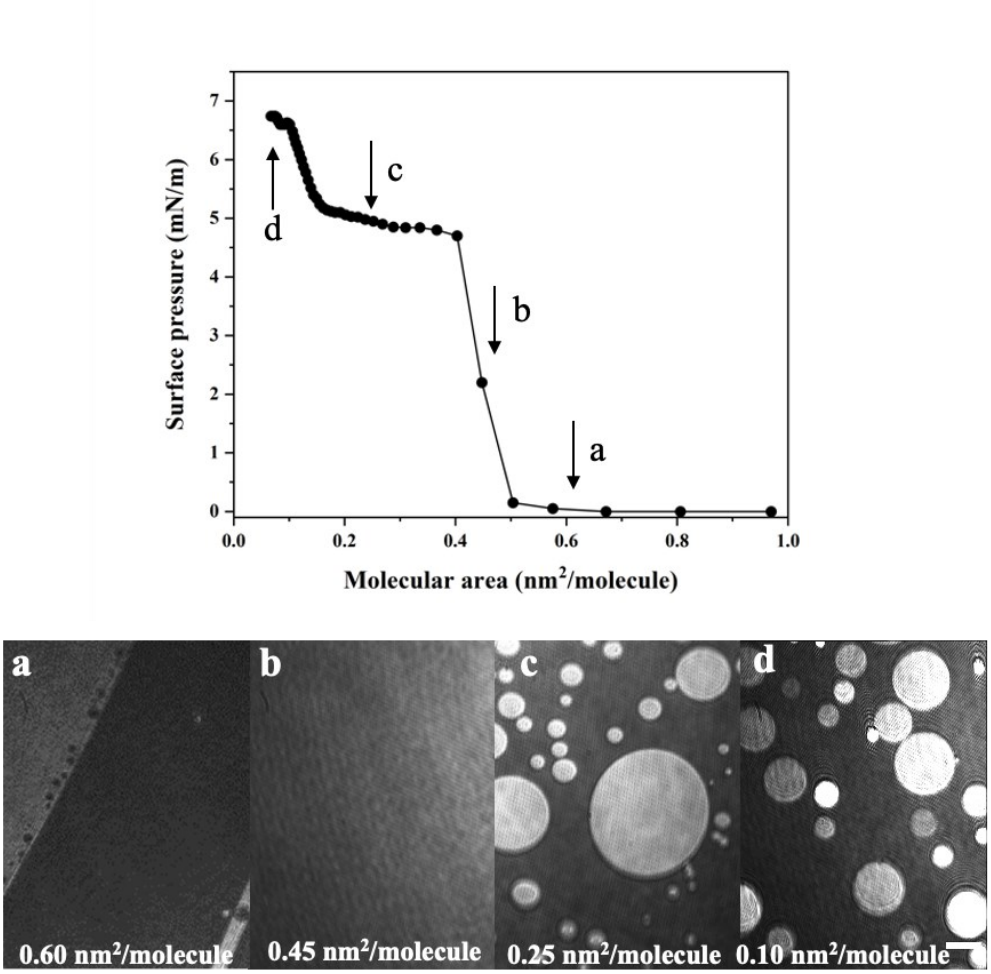

FIG. 4. Isotherm surface pressure coupled with BAM images as a function of molecular area of 8CB film at the air-water interface at T=20.0±0.1℃. Letters a-d indicate different regions at which the corresponding BAM images were recorded. Scale bare 200μm. The contrast between coexisting domains was maximized for clarity. The background intensity of (d) corresponds to the brightest domains in (c).

Both the surface tension of water $\gamma_0(T)$ and the surface tension of the 8CB-coated water decrease with temperature. FIG. 5 plots the surface pressure, defined as

$$\pi(T) = \gamma_0(T) - \gamma(T) \quad , \tag{8}$$

as a function of temperature in the 8CB trilayer/monolayer coexistence region at a mean molecular area of 0.30 nm^2/molecule, near the center of the quasi-plateau in Figure 4.

As shown in the Figure 5, the surface pressure decreases (interfacial tension increases) with temperature, but only by ~0.4 mN/m over the temperature range 20-50℃. The slope of $d\pi/dT$ is approximately -0.017 mN/m per degree Celsius, which implies a negative surface excess entropy.

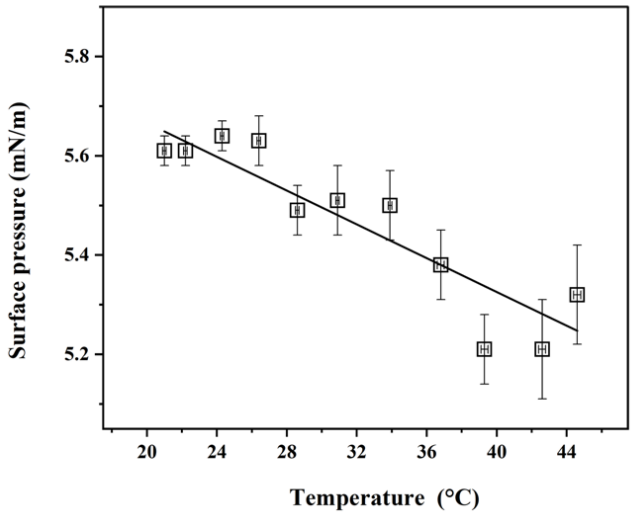

FIG. 5: Surface pressure at constant surface concentration (0.30 nm^2/molecule) plotted against temperature.

A similar negative temperature coefficient of surface pressure , implying a negative surface excess entropy, has been found for the surface-active polymer poly(dimethylsiloxane) (PDMS) at the air-water interface at different molecular areas [39]. For the region corresponding to trilayer/monolayer coexistence, the slope $(d\pi/dT)_{N,A}$ with respect to number of molecules and molecular area was ~ -0.1 mN/m per degree whereas the slope was less negative, approximately -0.05 mN/m per degree Celsius in the monolayer regime. The difference in the negative excess surface entropy for different molecular areas also suggests that the surface entropy of PDMS increases with decreasing surface area [39].

The measured negative surface excess entropy of 8CB on water is small. However, it would be interesting to connect this negative excess entropy to the microscopic structure of the monolayer. According to BAM images, the layer structures were nearly constant over the whole temperature range, with no significant change in the reflectivity for either the trilayer domains or the monolayer background. The domain brightness was very stable, with a standard deviation of less than 3%, over a temperature range in which bulk 8CB undergoes a phase transition from crystal to smectic and to nematic phases.

F. The line excess entropy

Here we report line tension measurements for the boundary between trilayer and monolayer phases in an 8CB Langmuir film at the air-water interface over the temperature range 10-45°C. The line tension of a single isolated domain is extracted from the characteristic relaxation time, the subfluid (water) viscosity, and the domain area through Eq. (7).

FIG. 6 shows the measured values of line tension as a function of temperature of the subfluid, with associated error estimations. The error bars arise from the uncertainties in the measurements of the domain area, viscosity of water and characteristic time, dominated by the first of these. We collected the data points under different experimental conditions, to test the reliability of the measurements. We used two different troughs: a KSV Inc. solid Teflon™ minitrough, which could be used for temperatures up to 30° C (after which the Teflon tends to delaminate from the aluminum base) and a homemade Teflon™-coated aluminum circular trough with cover, which could be used in the temperature range 20-50℃. We also used two different sources for the 8CB. If even trace contaminants, from either the troughs or the sample, are line active, they would concentrate at the monolayer/trilayer boundary and change its line tension. Any line active agents are unlikely to be the same, in identity and concentration, in the different sources

of 8CB material or leaching from the different troughs. The green diamond, blue hexagon and black square data points correspond to data using the Teflon Minitrough with sample 1 and the circular trough with sample 1 and 2, respectively. The observation that these two sources and two troughs all lead to the same line tension suggests that any impurities, if present, are not line active. Red circular data points with sample 3 corresponds to data with the circular trough covered, to test for any effect of humidity [40]. With the cover on, the humidity approaches 100%, while room humidity was 40-70 %. It is conceivable that low humidity can drive evaporation which can disturb the hydrodynamics of domain relaxation, which would yield inaccurate values for the line tension. Within experimental accuracy, the humidity does not appear to influence the apparent line tension.

Within the scatter, the line tension vs. temperature curve is linear, without clear jumps or changes in slope as the 8CB bulk phase transitions from crystalline to smectic to nematic. However, as temperature increases, so does the scatter in the line tension values, as seen in Figure 6. The Root Mean Square Deviation (RMSD) from the fit and the percentage deviation in two regions: $T \leq 25℃$ and $T \geq 30℃$ are $\sim \pm$ 0.73, 4% and $\pm$ 2.5, 11%, respectively. This scatter appears primarily for two reasons. One is due to difficulty in producing sufficiently isolated domains to avoid hydrodynamic effects from neighboring domains, which can either slow or speed up relaxation depending on domain relative position and orientation. Second, convection causes more movement in the subfluid at higher temperatures. Domains moving during the relaxation process can add strain in either direction.

Where bulk 8CB would undergo a phase transition from the nematic to the isotropic phase, at 40.5℃, isotropic droplets begin to appear, as shown in FIG 7. As the temperature of the subphase is increased above this transition temperature, holes begin to form in the trilayer domain, with brighter droplets at the edge. At higher temperatures, only large three-dimensional droplets are

observed. Thus, the trilayer begins to dewet the monolayer-covered surface starting approximately at the bulk isotropic phase transition temperature.

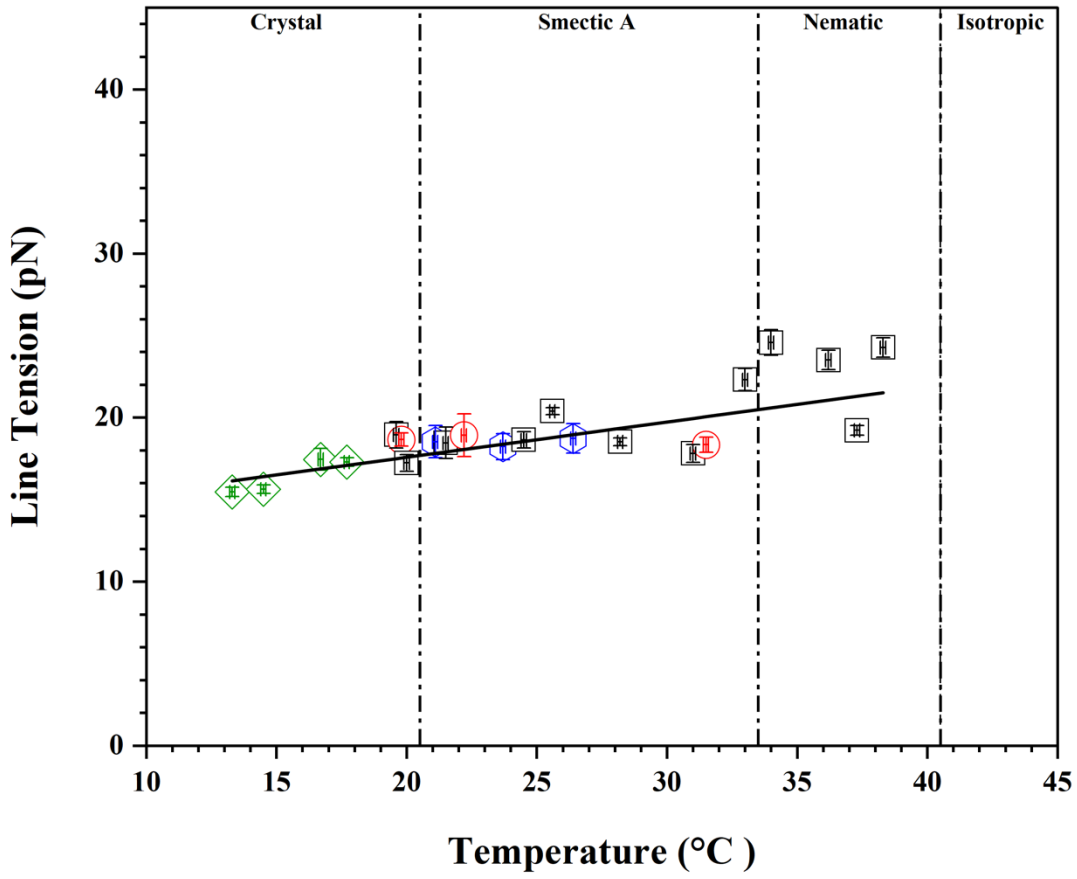

FIG. 6. The line tension vs. temperature under four different experimental conditions, with two troughs and two different samples. Sample 1 is from Sigma-Aldrich, with concentration 0.204 mg/ml, sample 2 from BDH Ltd with concentration 0.30 mg/ml and sample 3 is also from this source with concentration 0.27 mg/ml. Green diamond: sample 1 and solid minitrough; Black squares: Teflon-coated aluminum trough and sample 2; Blue hexagons: sample 1 with Teflon-coated aluminum trough; Red circles: sample 3 with a cover on the circular trough to increase humidity. Vertical lines indicate phase transition temperatures in bulk 8CB.

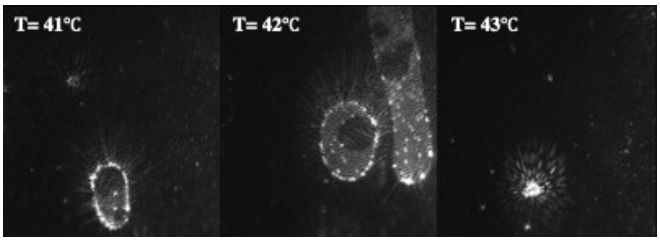

FIG. 7. Trilayer domains dewetting off the monolayer, above 40℃.

We interpret the line tension vs. temperature in terms of an excess line entropy for the boundary through Eq.(6), with the slope of the best fit through the line tension data points representing the average entropy per unit length of the boundary:

$$\frac{S^l}{L} = -\frac{d\lambda}{dT} = -0.21 \pm 0.01 \frac{pN}{℃} \tag{9}$$

Note that the entropy is constant within the uncertainties over the temperature range 10-50℃. However the positive slope of the line tension with temperature indicates that the specific excess entropy associated with line boundary is negative. A negative entropy is a priori unexpected. In principle an excess entropy can have either sign, while retaining the overall positive entropy for the system. However, it requires careful consideration.

III. DISCUSSION AND CONCLUSIONS

Here, we measured the line tension of the boundary of two coexisting phases with uncertainty ~1%. We observed a low value for the surface pressure temperature coefficient, which suggests that the layers remain well-defined. We studied the influence of the temperature on the line tension measurements to deduce the excess line entropy associated with trilayer/monolayer coexistence as:

$$S^L = -0.21 \pm 0.01 \frac{\mathrm{pN}}{℃}$$

This unusual behavior also has been found for surface tension [41-44]. The interfacial tension of a conventional interface between two isotropic liquids normally decreases with increasing the temperature, implying a positive surface excess entropy. However, negative surface entropies have been reported for the interface between a gas and a liquid crystal, and between a liquid crystal and an immiscible isotropic liquid. Gannon and Faber [41] found that the surface tension, measured by the Wilhelmy plate, of 5CB and 8CB in air is an increasing function of temperature below and above the N-I transition, with a discontinuity at the transition. Careful measurements by Tintaru et al. [42] using a static pendant drop method also found such a positive temperature coefficient for the surface tension of 8CB in air. The implied negative surface excess entropy of these liquid crystals is thought to be caused by excess orientational/positional order of the molecules near the surface compared to that in bulk [42].

Further Rai et al. [43] report, using a pendant drop measurement, that the surface tension between 5CB and PDMS increases with temperature. Kim et al [44], using similar methods, also observed an increase in the interfacial tension between water and 5CB in the presence of an adsorbed surfactant cetyltrimethylammonium bromide (CTAB) when passing through the N-I transition. All these reports suggest that, for the region below the N-I transition, the homeotropic ordering of liquid crystal at the interface causes a negative surface excess entropy as the nematic order parameter decreases. These measurements are also in agreement with a Monte Carlo calculation [45] of interfacial tension between a thermotropic liquid crystalline polymer and a flexible polymer. Above the N-I transition, these authors suggest an excess nematic or smectic order at the interface beyond the bulk transition [41-45].

In general, a negative excess surface entropy is associated with increased order at the surface compared to the bulk phase. Our results of a negative excess line entropy thus suggest

similar effects. It is difficult to imagine increased positional order at the boundary line of the same kind induced by a surface. However, the asymmetry between the inside and the outside of the domain could induce an excess tilt in one direction, analogous to a smectic C phase. A smectic C phase is more ordered than a smectic A phase, which is the only macroscopic smectic phase observed in 8CB films. The negative line entropy, implied by the increase of line tension with increasing temperature, thus suggests such a tilt.

More microscopic information would be required to test this hypothesis. Experimental techniques such as cryo-Transmission Electron Microscopy, Atomic Force Microscopy, or (with sufficient resolution), x-ray scattering microscopy [46-48] are conceivable but difficult on these types of systems, where domain edges may be millimeters apart but on the nanometer scale. It would be interesting to develop a molecular dynamics simulation of such liquid crystal films at the air-water interface to explore such hypotheses for molecular structure and organization at the boundary line. Such modeling would require a carefully defined Gibbs dividing surface between the 8CB and water surface and Gibbs dividing line between the two different phases within the surface.

IV. ACKNOWLEDGMENT

This work was supported by NSF DMR-1709985 and performed partly while EKM served at the National Science Foundation. HA was also supported by a scholarship from King Saud University. We thank Hiroshi Yokoyama for very useful discussions of negative surface and excess entropies in liquid crystalline systems.

V. REFERENCES

[1] A. R. Honerkamp-Smith, P. Cicuta, M. D. Collins, S. L. Veatch, M. den Nijs, M. Schick and S. L. Keller, Biophys. J. **95**, 236 (2008).

[2] R. Brewster, P. A. Pincus and S. A. Safran, Biophys. J. **97**, 1087 (2009).

[3] P. Dhar, E. Eck, J. N. Israelachvili, D. W. Lee, Y. Min, A. Ramachandaran, A. J. Waring and J. A. Zasadzinski, Biophys. J. **102**, 56 (2012).

[4] A. A. Bischof and N. Wilke, Chem. Phys. Lipids **165**, 737 (2012).

[5] B. L. Stottrup, A. M. Heussler and T. A. Bibelnieks, J. Phys. Chem. B **38**, 11091 (2007).

[6] B. L. Stottrup, J. TigreLazo, V. B. Bagobza, J. C. Kunz and J. A. Zasadzinski, Langmuir **35**, 16053 (2019).

[7] M. Fauquignon, E. Ibarboure and J. F. Le Meins, Biophys. J. **121**, 61 (2022).

[8] J. Pusterla, J. M. Hernández, N. Wilke, E. Schneck and R. G. Oliveira, Colloids Surf. B **207**, 112027 (2021).

[9] T. A. Enoki, J. Wu, F. A. Heberle and G. W. Feigenson, Biochim. Biophys .**1863**, 183586 (2021).

[10] K. Simons and E. Ikonen, Nature **387**, 569 (1977).

[11] D. Lingwood and K. Simons, Science **327**, 46 (2010).

[12] S. P. Rayermann, G. F. Rayermann, C. E. Cornell, A. J. Merz and S. L. Keller, Biophys. J. **113**, 2425 (2017).

[13] E. Sezgin, I. Levental, S. Mayor and C. Eggeling, Nat. Rev. Mol. Cell Biol **18**, 361(2017).

[14] J. A. Nieto-Garai, M. Lorizate and F. X. Contreras, BBA. Biochim. Biophys. **1864**, 183813,(2022).

[15] D. J. Benvegnu and H. M. McConnell, J. Phys. Chem. **96**, 6820 (1992).

[16] I. Sriram and D. K. Schwartz, Surf. Sci. Rep. **67**, 143 (2012).

[17] H. A. Stone and H. M. McConnell, Proc. R. Soc. London, Ser. A **448**, 97 (1995).

[18] R. M. Weis and H. M. McConnell, Nature **310**, 47 (1984).

[19] D. J. Keller, H. M. McConnell and V. T. Moy, J. Phys. Chem. **90**, 2311 (1986).

[20] E. K. Mann, S. Henon, D. Langevin, J. Meunier and L. Leger, Phys. Rev. E **5**, 5708 (1995).

[21] J. Läuger, C. R. Robertson, C. W. Frank and G. G. Fuller, Langmuir **12**, 5630 (1996).

[22] L. Zou, J. Wang, P. Banset and E. K. Mann, Phys. Rev. E **76**, 031602 (2007).

[23] J. C. Geminard, C. Laroche and P. Oswald, Phys. Rev. E **58**, 5923 (1998).

[24] A. Zywocinski, F. Picano, P. Oswald and J. C. Geminard, Phys. Rev. E **62**, 8133 (2000).

[25] J. C. Alexander, A. J. Bernoff, E. K. Mann, J. A. Mann, Jr., J. R. Wintersmith and L. Zou, J. Fluid Mech. **571**, 191 (2007).

[26] J. C. Alexander, A. J. Bernoff, E. K. Mann, J. A. Mann, Jr., J. R. Wintersmith and L. Zou, Phys. Fluids. **18**, 062103 (2007).

[27] J. R. Wintersmith, L. Zou, A. J. Bernoff, J. C. Alexander, J. A. Mann, Jr. and E. K. Mann, Phys. Rev. E **75**, 061605 (2007).

[28] A. W. Adamson and A. P. Gast, Physical Chemistry of Surfaces, 6th ed. (John Wiley & Sons, Inc., New York, 1997)

[29] R. S. Hansen, J. Phys. Chem. **66**, 410 (1961).

[30] L. A. Turkevich and J. A. Mann, Jr., Langmuir **6**, 457 (1990).

[31] J. S. Yarzebinski, MS Thesis, Kent State University, 2016.

[32] H. A. Alwusaydi, MS Thesis, Kent State University, 2017.

[33] M. N. de Mul and J. A. Mann, Jr., Langmuir **14**, 2455 (1998).

[34] J. Wang, L. Zou, A. Jákli, W. Weissflog and E. K. Mann, Langmuir **22**, 3198 (2006).

[35] S. Hénon and J. Meunier, Rev. Sci. Instrum. **62**, 936 (1991).

[36] M. N.de Mul and J. A. Mann, Jr., Langmuir **10**, 2311 (1994).

[37] K. Inglot, T. Martynski and D. Bauman, Liq. Cryst. **33**, 855 (2006).

[38] A. Modlinska, K. Inglot, T. Martynski, R. Dabrowski, J. Jadzyn and D. Bauman, Liq. Cryst. **36**, 197 (2009).

[39] S. Granick, S. J. Clarson, T. R. Formoy and J. A. Semlyen, Polymer **26**, 925 (1984).

[40] E. K. Mann, S. , Hénon, D. Langevin and J. Meunier, J. Phys. II France **2**, 1683 (1992).

[41] M. G. J. Gannon and T. E. Faber, Philosophical magazine A **37**, 117 (1987).

[42] M. Tintaru, R. Moldovan, T. Beica and S. Frunza, Liq. Cryst. **28**, 793 (2001).

[43] P. K. Rai, M. M. Denn and C. Maldarelli, Langmuir **19**, 7370 (2003).

[44] J. W. Kim, M. Lee and J. J. Megda, Langmuir **20**, 8110 (2004).

[45] X. Li and M. M. Denn, Macromolecules **35**, 6446 (2002).

[46] M. Kutsal, H. F. Poulsen, G. Winther, H. O. Sørensen, and C. Detlefs, Appl. Cryst **55**, 1125-1138 (2022)

[47] F. Berenguer, G. Pettinari, M. Felici, N. Balakrishnan, J. N. Clark, S. Ravy, A. Patané, A. Polimeni and G. Ciatto, Commun Mater **1**, 19 (2020).

[48] H. N. Chapman and K. A. Hugent, Nature Photon **4**, 833-839 (2010).